Dielectric to pyroelectric phase transition induced by defect migration

2015 New J. Phys. 17 023036

(http://iopscience.iop.org/1367-2630/17/2/023036)

New Journal of Physics
The open access journal at the forefront of physics

Deutsche Physikalische Gesellschaft DPG
IOP Institute of Physics

Published in partnership with: Deutsche Physikalische Gesellschaft and the Institute of Physics

OPEN ACCESS

RECEIVED
9 October 2014

REVISED
21 November 2014

ACCEPTED FOR PUBLICATION
25 November 2014

PUBLISHED
10 February 2015

PAPER

Dielectric to pyroelectric phase transition induced by defect migration

Juliane Hanzig[1,*], Erik Mehner[1,*], Sven Jachalke[1], Florian Hanzig[1], Matthias Zschornak[1,2], Carsten Richter[1,3], Tilmann Leisegang[4], Hartmut Stöcker[1] and Dirk C Meyer[1]

[1] Institut für Experimentelle Physik, TU Bergakademie Freiberg, Leipziger Straße 23, 09596 Freiberg, Germany
[2] Institut für Ionenstrahlphysik und Materialforschung, Helmholtz-Zentrum Dresden-Rossendorf, Bautzner Landstraße 400, 01328 Dresden, Germany
[3] Deutsches Elektronen-Synchrotron, Photon-Science, Notkestraße 85, 22607 Hamburg, Germany
[4] Fraunhofer-Technologiezentrum Halbleitermaterialien, Am St.-Niclas-Schacht 13, 09599 Freiberg, Germany
[*] These authors contributed equally to this work.

E-mail: erik.mehner@physik.tu-freiberg.de

Keywords: pyroelectricity, defect migration, phase transition

Supplementary material for this article is available online

Abstract

Subjecting strontium titanate single crystals to an electric field in the order of 10^6 V m^{-1} is accompanied by a distortion of the cubic crystal structure, so that inversion symmetry vanishes and a polar phase is established. Since the polar nature of the migration-induced field-stabilized polar (MFP) phase is still unclear, the present work investigates and confirms the pyroelectric structure. We present measurements of thermally stimulated and pyroelectric currents that reveal a pyroelectric coefficient p_{MFP} in the order of 30 μC K^{-1}m^{-2}. Therefore, a dielectric to pyroelectric phase transition in an originally centrosymmetric crystal structure with an inherent dipole moment is found, which is induced by defect migration. From symmetry considerations, we derive space group $P4mm$ for the MFP phase of $SrTiO_3$. The entire electroformation cycle yields additional information about the directed movement and defect chemistry of oxygen vacancies.

1. Introduction

Pyroelectric and piezoelectric materials have become increasingly important for practical applications beyond infrared sensor technology [1]. Promising advances in waste heat recovery [2–4], x-ray generation [5], and disinfection [6] employ the pyroelectric effect. The prerequisite of a non-centrosymmetric structure is fulfilled by inorganic single crystals [7], polymers [8], composite films [9], and ceramics [10]. However, a comparatively new fundamental approach is based on centrosymmetric materials, which respond to an external influence such as mechanical strain gradients [11] or electric fields [12] by symmetry breaking.

Strontium titanate is a well-known model transition metal oxide, which is diversely used and under permanent research for use as high-k dielectric [13], resistive random access memory [14–16], battery [17], oxygen sensor [18], superconductor [19], or photocatalytic material [20]. Its perovskite aristotype structure is comparatively stable, as verified by the Goldtschmidt tolerance factor [21]. Crystallizing in the cubic perovskite structure within space group $Pm\bar{3}m$, dielectric $SrTiO_3$ [22, 23] undergoes several phase transitions during temperature decrease. Below 110 K [24, 25], a tetragonal distortion occurs, leading to a so-called antiferrodistortive (AFD) phase, still showing inversion symmetry within space group $I4/mcm$. Further decrease in temperature initiates a ferroelectric phase transition at $T_c = 40$ K, which remains ever incomplete, down to 0 K [26]. Therefore, intensive investigations on ferroelectricity in strontium titanate [27] caused by temperature decrease, as well as symmetry breaking, have been undertaken: grain boundaries in ceramics [28], enhanced point defect concentrations effecting polar microregions [29] in single crystals, or strain and stress in thin films [30]. Furthermore, ferroelectricity has been found at room temperature by Haeni *et al* [31] in

homogeneously strained thin films and by Ehre *et al* [32], who discovered piezo- and pyroelectric phases in quasi-amorphous thin films.

Recently, a migration-induced field-stabilized polar (MFP) phase in $SrTiO_3$ single crystals at room temperature has been reported [12], which is caused by an electroformation process using an electric field of 10^6 V m^{-1}. Combining these experimental findings of broken inversion symmetry with the reversibility of the phenomenon, albeit on a time scale of hours, the requirements for ferroelectricity are fulfilled. Nonetheless, the new MFP phase cannot be regarded as ferroelectric as defined in the literature [33, 34], because the polarization is sustained and aligned by the external electric field. The proposed model implies piezoelectric and polar properties allowing pyroelectricity but no experimental evidence has been provided. If the MFP phase was pyroelectric, the number of possible space groups for its structure prediction would be significantly reduced.

Consequently, we present an investigation of the pyroelectric properties of the MFP phase of $SrTiO_3$ confirming its pyroelectricity. Furthermore, the impact of oxygen vacancy migration on the phase transition through thermally stimulated current measurements are presented.

2. Materials and methods

All investigated (001) orientated strontium titanate single crystals were $5 \times 5 \times 0.1$ mm^3 in size and purchased from CrysTec GmbH, Berlin. To obtain well-defined TiO_2-terminated surfaces, an etching process was executed followed by a temperature treatment [12]. For electrical measurements, planar front- and backside 4×4 mm^2 contacts of 50 nm titanium were deposited by magnetron sputtering to yield ohmic behavior and avoid surface conductivity influences. Typical measurement techniques for pyroelectric properties, like the Byer–Roundy method [35], are unsuitable to characterize the MFP phase because they cannot distinguish between pyroelectric and thermally stimulated signals stemming from the thermal detrapping of charge carriers. Such a thermally stimulated current is to be expected as a constant background due to the constant refilling of traps by the external voltage in an electroformation experiment described in [12]. We therefore chose an adapted Sharp–Garn method [36, 37] to determine the pyroelectric coefficient p_z along a polar axis z to which several effects contribute:

$$p_z = \underbrace{p_{\mathrm{prim},z}}_{\text{primary}} + \underbrace{\varepsilon_0 E_k \frac{\partial \varepsilon_{zk}}{\partial T}}_{\text{field-induced}} + \underbrace{\frac{\partial d_{zkl}\sigma_{kl}}{\partial T}}_{\text{secondary}} + \underbrace{\frac{\partial \mu_{zijk}\frac{\partial u_{ij}}{\partial r_k}}{\partial T}}_{\text{flexoelectric}} + \cdots \tag{1}$$

with permittivity tensor ε_{zk}, external electric field E_k, piezoelectric tensor d_{zkl}, stress tensor σ_{kl}, flexoelectric tensor μ_{zijk}, and strain tensor u_{ij}. The Sharp–Garn method is based on a low frequency sinusoidal temperature excitation of the sample

$$T(t) = T_0 + T_A \cdot \sin\left(\omega t + \varphi_T\right) \tag{2}$$

with temperature amplitude T_A, angular frequency ω, offset temperature T_0, and phase offset φ_T. The current response to this excitation is composed of pyroelectric current i_{PE} and non-pyroelectric current i_{nPE}

$$i_{\mathrm{PE}}(T) = p_z(T) A \frac{\mathrm{d}T}{\mathrm{d}t}, \quad i_{\mathrm{nPE}}(T) = i_{\mathrm{nPE},0} + B \cdot T \tag{3}$$

with temperature-independent thermally stimulated current $i_{\mathrm{nPE},0}$ at T_0 and temperature-dependent i_{TSC} coefficient $B(T)$ describing the nature of the thermal traps discharged by the temperature excitation [36, 37]. The expression for i_{nPE} holds for small ($\approx$1 K) temperature excitations. Now the overall time- and temperature-dependent current response i can be written as follows

$$i = i_{\mathrm{nPE},0} + BT_0 + BT_A \sin(\omega t) + p_z \cdot AT_A\omega \cos(\omega t) = i_{\mathrm{DC}} + i_{\mathrm{th}} \cdot \sin\left(\omega t + \varphi_i\right) \tag{4}$$

with electrode area A and the overall phase shift $\varphi = \varphi_T - \varphi_i$ between the temperature sine wave and the current response. Thus, the current response i is split into a time-constant part i_{DC} and a time-dependent part with the amplitude i_{th}. The non-modulated part of the current response i_{DC} is, in this kind of experiment, dominated by the contribution of the electroformation i_{F}. With equations (3) and (4), the pyroelectric coefficient can be extracted from a measurement of the thermal current response amplitude i_{th} and phase shift φ of the current response as

$$p_z = \frac{i_{\mathrm{th}} \sin\varphi}{A \cdot T_A \cdot \omega}. \tag{5}$$

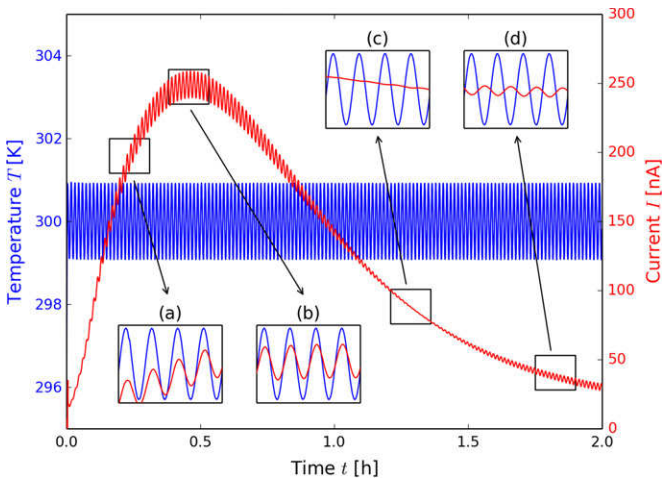

Figure 1. Current response i of a $SrTiO_3$ single crystal during electroformation using an external electric field of 10^6 V m^{-1} superimposed by a sinusoidal temperature excitation: (a)–(b) in-phase current-temperature behavior during oxygen vacancy migration, (c) disappearance of temperature-induced modulation of current response, and (d) reversed sign in-phase current-temperature behavior when defect separation is finished and the MFP phase is established. Same current scale for all insets highlights amplitude changes in i_{th}.

The original technique is extended here by applying an external electric field during the entire measurement required for the electroformation process. The sample temperature is measured using a Pt100 resistive thermometer placed directly adjacent to the sample. Temperature control is achieved with a software-based closed-loop proportional-integral-derivative (PID) controller that samples the thermometer through a multimeter. The electrical signal from the sample connected in series with the high voltage source is recorded using an electrometer. Sandwiched between two copper contact plates, the sample is held in place with a fixture to keep the strain constant.

The data evaluation decomposes the measured current from the sample into the thermal current response i_{th} and the current base line i_F caused by the electroformation process. The latter is obtained by smoothing out the oscillatory part using a uniform moving window average whose width coincides with the temperature excitation period $\tau = \frac{2\pi}{\omega}$. Subsequently, the Fourier components of the oscillatory signal $i_{th}(t)$ and the temperature signal $T(t)$ corresponding to this period (i. e., $\varphi_i, \varphi_T, i_{th}, T_A$) are calculated for each interval by direct integration.

All investigated samples revealed equal qualitative behavior, but quantitative results depended on the crystal real structure and, hence, differed slightly for each specimen.

3. Results

3.1. Qualitative thermal current analysis

Figure 1 shows the current response i of a $SrTiO_3$ single crystal during electroformation when applying an external electric field of 10^6 V m^{-1} superimposed by a sinusoidal temperature excitation. An offset temperature of $T_0 = 300$ K and an amplitude of $T_A = 1$ K were used for oscillating temperature at different angular frequencies ω. The time-dependent forming current i_F is composed of ionic and electronic parts, which are attributed to oxygen vacancy migration [12, 16, 38, 39]. The characteristic shape of the electronic part is a current increase up to a maximum followed by a decrease with a similar slope down towards the initial current value. In addition, the forming current i_F is superimposed by the oscillatory thermal current response i_{th}. Regarding i_{th}, four different ranges (see insets (a)–(d) of figure 1) have to be distinguished:

At the beginning of the electroformation i_{th} shows an in-phase temperature behavior (see figure 1, inset (a) and (b)) typical for semiconductors. Heating ($\partial T/\partial t > 0$) results in a current increase, whereas cooling ($\partial T/\partial t < 0$) leads to a current decrease. Intrinsic defects like oxygen vacancies $V_O^{\cdot\cdot}$, given here in Kröger–Vink notation [40], cause additional bandgap states near the conduction band [41], which are charged and discharged when temperature oscillates and, thus, contribute to the thermally stimulated current i_{TSC}. This behavior is correlated with defect migration, especially of oxygen vacancies due to the higher diffusion coefficient compared to strontium vacancies. Coinciding with the peak of i_F, the amplitude maximum of i_{th} depicts the largest number of moving defects. Subsequently, more and more defects arrive at the cathode, leading to the formation of the MFP phase at the anode and a decrease of i_{th} (see figure 1, inset (c)). When defect migration is declining, an out-of-phase current contribution in i_{th} can be detected, revealing the temperature dependence on an inherent polarization P_{MFP} of the formed MFP phase [12]. With a successful formation of the MFP phase in the single

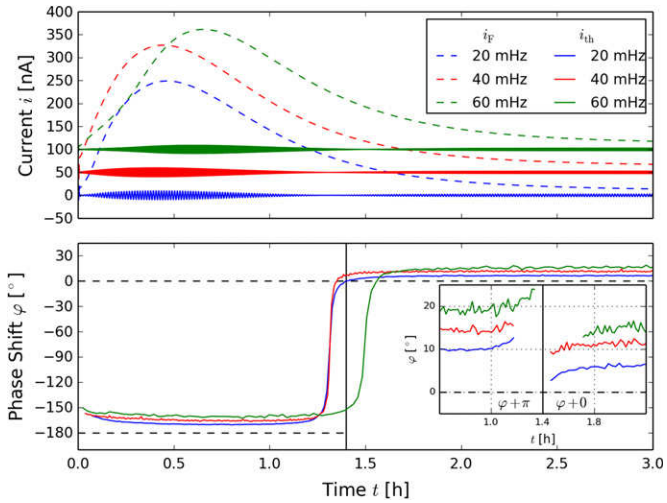

Figure 2. Electroformation of a $SrTiO_3$ single crystal in an external electric field of 10^6 V m^{-1} superimposed by a sinusoidal temperature excitation with different frequencies: decomposition of time-dependent current i into forming current i_F and thermal current i_{th} (top), data sets are shifted by 50 nA for each frequency. Time-dependent phase shift of pyroelectric current response (bottom). The inset shows phase shift behavior at the transition point which was adjusted by π before the transition to emphasize the change in pyroelectricity.

crystal, the thermal current response shows a major phase shift of π, indicating metallic conductivity (see figure 1, inset (d)). Accordingly, heating ($\partial T/\partial t > 0$) results in current decrease, whereas cooling ($\partial T/\partial t < 0$) leads to a current increase. This effect is caused by the accumulation of oxygen vacancies at the cathode, leading to a highly conductive area, known as the virtual cathode [16]. Here, the defect clusters form an electronic mid-bandgap state [42] deep enough to trap electrons, which quenches i_{TSC} (compare insets of figure 1). It should be noted that this metallic signature stems most likely from the virtual cathode alone, whereas the conduction regime in the remaining crystal volume does not change. Conversely, the conductivity of the defect depleted anode region is expected to drop and thus the overall conductivity of the sample does not change significantly.

Another important detail is the development of the amplitude of i_{th} during electroformation (see insets of figure 1). At the beginning, a comparatively small amplitude evolves into a higher one at maximum i_F, where formation of the MFP phase proceeds. The maximum amplitude of i_{TSC} marks the largest number of mobile oxygen vacancies in the whole bulk single crystal coinciding with the maximum of i_F. Subsequently, when the current amplitude i_{TSC} vanishes, the metallic current contribution equals the semiconducting one. At this time the oxygen redistribution can be regarded as nearly complete. The metallic behavior of the recurring amplitude is in accordance with the oxygen vacancy accumulation at the virtual cathode [16]. Conversely, the oxygen vacancy clustering creates a defect band lowering the thermal excitability of the oxygen vacancies [42, 43] (see figure 4(b)).

Further experiments show the independence of i_{th} and i_F on the polarity of the external electric field underlining the non-ferroelectric character. The external electric field aligns the oxygen vacancy migration and therefore the polarization. In summary, this kind of measurement is suitable to track the movement of charged mobile defects in oxides.

3.2. Pyroelectricity

Extracting the pyroelectric coefficient from the performed measurements deserves discussion of different pyroelectric contributions (see equation (1)): first, the primary pyroelectric coefficient $p_{prim,z}$ caused by the permanent dipole moment of the MFP phase; second, the temperature dependency of the dielectric constant ε_{zk} in an external electric field E_k; third, mechanical influences may cause polarization changes through the piezoelectric and flexoelectric effects. We neglect secondary and higher-order pyroelectric effects because the samples were measured at constant strain. Further, centrosymmetric strontium titanate shows no piezoelectricity and the lattice parameter changes observed during the evolution of the MFP phase occur on a significantly longer timescale than the thermal excitation [12]. Using literature data [11] for $\mu_{[001]}$, we estimate two orders of magnitude lower flexoelectric polarization resulting from the temperature excitation than observed. Hence, only primary and electric field induced pyroelectricity must be considered.

Figure 2 pictures the phase shift $\varphi(t)$ of the thermal current response of a $SrTiO_3$ single crystal during electroformation with respect to the temperature excitation sine wave for different frequencies. It can be clearly seen that the higher the thermal excitation frequency, the more phase shift occurs, which distinctively indicates

Table 1. Relation of temperature excitation frequency with phase shift of pyroelectric current at times before and after electroformation and resulting pyroelectric coefficients.

Excitation frequency ω	Phase shift φ(0.7 h)	Phase shift φ(2.6 h)
20 mHz	−170.56°	−173.93°
40 mHz	−165.75°	−169.05°
60 mHz	−160.94°	−164.48°
p_z [μCK^{-1}m^{-2}]	−177	−147

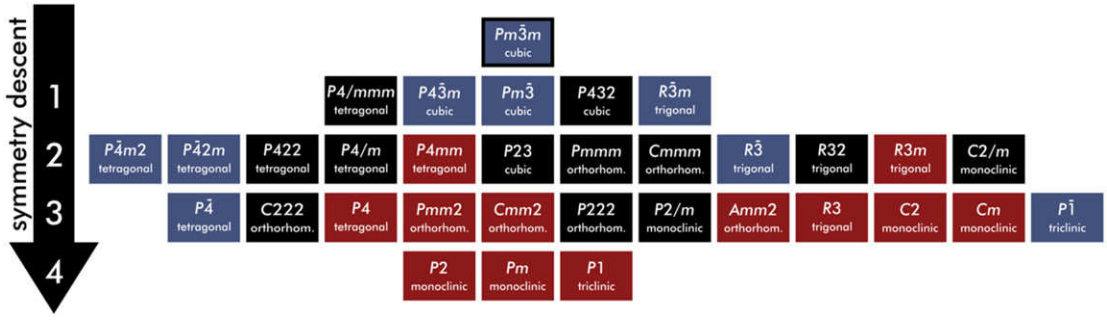

Figure 3. Translationsgleiche symmetry descents from space group $Pm\bar{3}m$. The actual transitions (descend, across, and back) are not shown for clarity. Blue color marks space groups with inversion symmetry, red color symbolizes pyroelectric space groups, and black color indicates non-pyroelectric space groups without inversion symmetry.

pyroelectricity. The major feature in $\varphi(t)$ is a change in phase shift of π at the crossing between dominating semiconducting and metallic behavior as marked in inset (c) of figure 1. The deviation in phase shift from −π in $\varphi(t)$ before the sign change is attributed to the field-induced pyroelectricity term in equation (1). If the phase shift by π in i_{th} is removed from $\varphi(t)$, it is obvious that $|p_z|$ is reduced by the formation of the MFP phase (see inset of figure 2). Therefore, $p_{\mathrm{prim},z}$ and $\varepsilon_0 E_k \partial\varepsilon_{zk}/\partial T$ differ in sign. However, this experiment is unable to distinguish absolutely between field-induced and primary pyroelectric effect of the MFP phase. Since both contributions are present and ε_{zz} is reported inversely proportional to temperature [44], we assume that $p_{\mathrm{prim},z}$ is positive and $\varepsilon_0 E_k \partial\varepsilon_{zk}/\partial T$ is negative. Based on the remaining phase difference before and after electroformation, a pyroelectric coefficient $p_{\mathrm{prim},z}$ of 30 μC K^{-1}m^{-2} can be obtained (see table 1). Positive pyroelectric coefficients are rarely found [45] and may be attributable to the field-stabilized nature of the MFP phase.

4. Discussion

4.1. Structure prediction for MFP phase

Based on the presented measurements, a coherent argumentation to predict the crystal structure of the MFP phase follows. Relying on literature data [12] and additional x-ray diffraction experiments, only translationsgleiche subgroups have to be considered for a symmetry descent from the cubic $Pm\bar{3}m$ of $SrTiO_3$. These 32 possible *t*-subgroups can be categorized into those with inversion center, pyroelectric and non-pyroelectric space groups without inversion symmetry (see figure 3). From the remaining twelve pyroelectric space groups, the seven with tri-, monoclinic, or trigonal symmetry can be strictly excluded [12] (see supplementary material). Ruling out the three orthorhombic space groups with a twofold rotation axis is not possible with certainty due to the diffraction geometry with hardly accessible *hk*0 reflections. A conceivable *P*4 configuration with AFD-like twisted oxygen octahedra prevents the primitive centering and therefore has an enlarged unit cell violating the requirement of a translationsgleiche symmetry descent. With the assumption of no Jahn–Teller distortion, space group *P*4 can be entirely excluded due to the apical position of titanium in the oxygen octahedron. Furthermore, structures with space group *P*4 are yet to be discovered in the perovskite familiy [46]. Thus, only *P*4*mm* remains, which is in good agreement with structure-field maps from the literature [45] reporting *P*4*mm* for $A^{2+}B^{4+}O_3$ perovskites. Consequently, all indications point to space group *P*4*mm*.

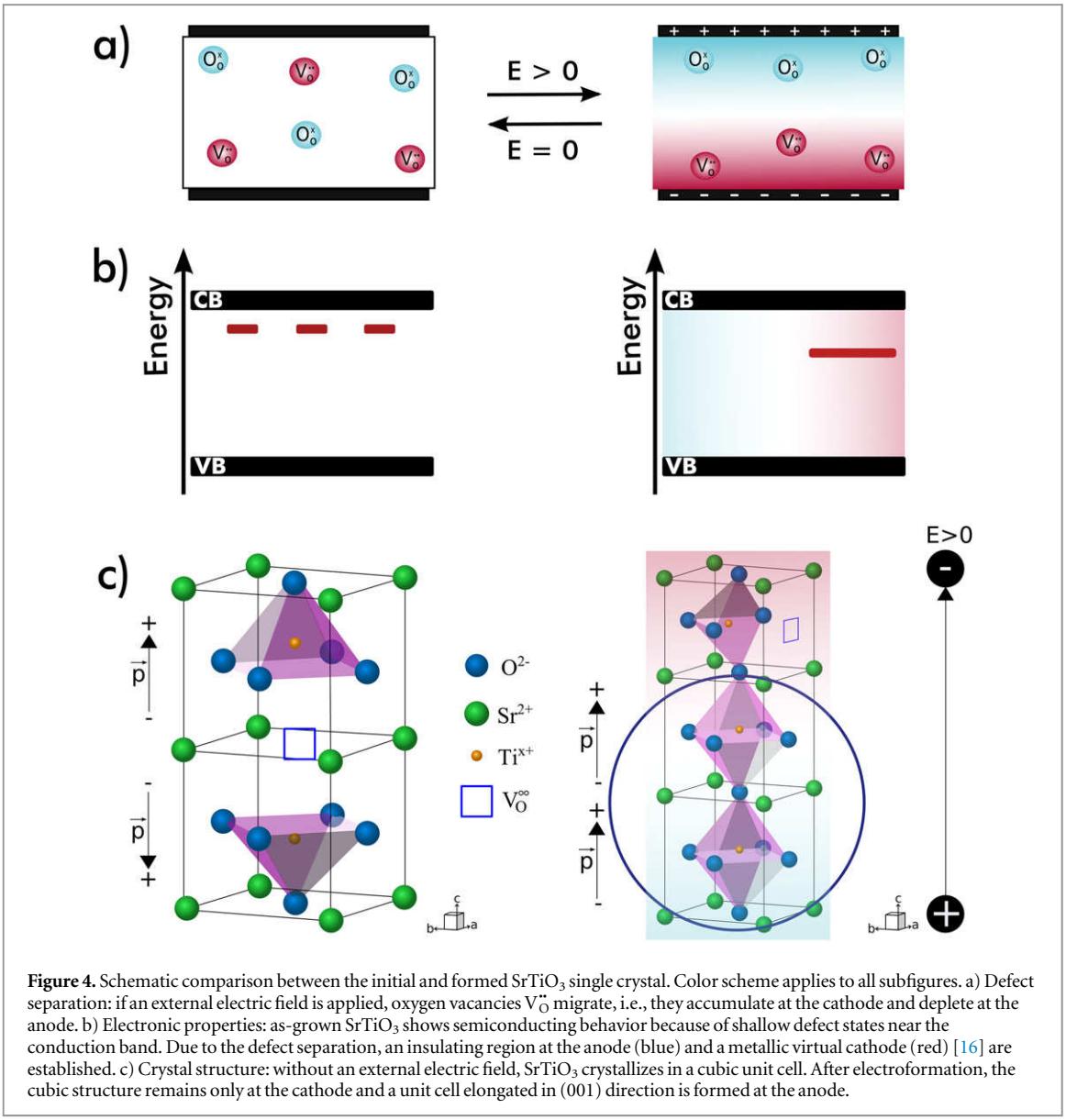

Figure 4. Schematic comparison between the initial and formed $SrTiO_3$ single crystal. Color scheme applies to all subfigures. a) Defect separation: if an external electric field is applied, oxygen vacancies $V_O^{\cdot\cdot}$ migrate, i.e., they accumulate at the cathode and deplete at the anode. b) Electronic properties: as-grown $SrTiO_3$ shows semiconducting behavior because of shallow defect states near the conduction band. Due to the defect separation, an insulating region at the anode (blue) and a metallic virtual cathode (red) [16] are established. c) Crystal structure: without an external electric field, $SrTiO_3$ crystallizes in a cubic unit cell. After electroformation, the cubic structure remains only at the cathode and a unit cell elongated in (001) direction is formed at the anode.

4.2. Dielectric to pyroelectric phase transition

Combining these findings, it is now possible to discuss the peculiarities of the phase transition of cubic $SrTiO_3$ into the MFP phase of $SrTiO_3$ in the framework of displacive or rotational [47] phase transitions of perovskites. In general, materials undergo structural phase transitions when intensive state variables like temperature or pressure are changed, e. g., all ferro- and pyroelectrics, such as $LiNbO_3$, $LiTaO_3$, and $BaTiO_3$, undergo a structural phase transitions when temperature passes the Curie temperature T_C. As for $SrTiO_3$, no complete ferroelectric phase transition occurs: the experimentally proven pyroelectricity in bulk $SrTiO_3$ at room temperature is unprecedented. In this material system, structural phase transitions can be created by stoichiometry changes; as for example, in the solid solution series of $Ba_{1-x}Sr_xTiO_3$, [48, 49] and $PbZr_{1-x}Ti_xO_3$ [47, 50]. In contrast, the reported phase transition does not rely on extrinsic doping but uses intrinsic defect engineering by defect migration. A delimitation regarding stress-induced phase transitions, which mainly occur in thin films [51], is unnecessary because of their small impact on secondary pyroelectricity (compare equation (1)). Furthermore, electric field induced phase transitions can be found in literature, where polar structures of oxides [52, 53] and polymers [54] are involved. Usually the external electric field is coupled to existing dipole moments. In contrast, the referred electric field induced dielectric to pyroelectric phase transition is characterized as a structural phase transition from an originally centrosymmetric into a polar structure. These experimental findings evidence the interaction of the electric field with charged species, e. g. defects like oxygen vacancies $V_O^{\cdot\cdot}$. Although Fleury *et al* [55] presented a field-induced phase transition in $SrTiO_3$ single crystals, it should be noted that their measurements were performed at such low temperatures, that the electric field is directly linked to soft phonon modes. Thus, this phase transition is to be categorized as a field-induced polar to polar phase transition. In our case, electrostrictive effects can be excluded since no experimental evidence for

lattice parameter changes were found besides the effects of defect migration (see supplementary data available at stacks.iop.org/njp/17/013052/mmedia). Consequently, a classification as a displacive phase transition by defect migration is appropriate.

To summarize the defect-chemical, structural, and electronic aspects of the phase transition into the MFP phase of $SrTiO_3$, the following model is presented (see figure 4): The initial state shows statistically distributed oxygen vacancies that move to the cathode when an electric field is applied. The electroformation is finished when defects are completely separated (see figure 4(a)). The MFP phase is established at the anode, where oxygen vacancies are depleted, causing defect free unit cells with an inherent dipole moment [12] (see figure 4(c)), which are responsible for the reported pyroelectricity. Analyzing the electronic situation during and after electroformation (see figure 4(b)), single oxygen vacancies form shallow energy states near the conduction band leading to the semiconducting behavior in the initial state. Through defect separation, oxygen vacancies leave the anode, making this area insulating, and cluster at the cathode, generating deep traps to build up a 'conduction band' for metallic conductivity, as shown in section 3.1. Besides, the polar nature of the MFP phase is confined to pyroelectric, because the dipole moments are not switchable without destroying the polar phase.

5. Conclusion

In summary, the field-induced redistribution of oxygen vacancies on $SrTiO_3$ causes a polar phase at the anode with a pyroelectric coefficient on the order of 30 $\mu C\ K^{-1}m^{-2}$ at room temperature, which is in the range of single crystal pyroelectric oxides, like lithium niobate. Consequently, a dielectric to pyroelectric phase transition is induced based on defect migration, which is accompanied by a symmetry breaking and the formation of an inherent dipole moment in an originally centrosymmetric crystal structure.

From the crystallographic point of view, the present work introduces a new concept to extend the material classes required for pyroelectricity by modifying centrosymmetric structures by defect engineering. Here, a crystal structure prediction for the MFP phase with spacegroup *P4mm* is presented. With this space group prediction and the already demonstrated field dependence of the lattice distortion of the MFP[12] phase, we expect the pyroelectric coefficient of the MFP phase to be tuneable by the external electric field once electroformation is concluded. Furthermore, it is demonstrated that pyroelectric measurement methods are suitable to track defects due to their electric characteristics.

Acknowledgments

This work has been performed in the joint research project CryPhysConcept — Mit Kristallphysik zum Zukunftskonzept elektrochemischer Energiespeicher (03EK3029A), which is financially supported by the Federal Ministry of Education and Research (BMBF). Part of this work has been done within the PyroConvert junior research group (100109976) that is financially supported by the European Union (European Regional Development Fund) and the Ministry of Science and Art of Saxony (SMWK). The research was partly done at the Rossendorf beamline BM20 at the ESRF. The authors acknowledge the kind support and funding of the ESRF.

References

[1] Lee M, Guo R and Bhalla A S 1998 *J. Electroceramics* **2** 229
[2] Olsen R B, Bruno D A and Briscoe J M 1985 *J. Appl. Phys.* **58** 4709
[3] Nguyen H, Navid A and Pilon L 2010 *Appl. Therm. Eng.* **30** 2127
[4] Navid A, Vanderpool D, Bah A and Pilon L 2010 *Int. J. Heat Mass Transfer* **53** 4060
[5] Rosenman G, Shur D, Krasik Y E and Dunaevsky A 2000 *J. Appl. Phys.* **88** 6109
[6] Gutmann E, Benke A, Gerth K, Böttcher H, Mehner E, Klein C, Krause-Buchholz U, Bergmann U, Pompe W and Meyer D C 2012 *J. Phys. Chem.* C **116** 5383
[7] Bartholomäus T, Buse K, Deuper C and Krätzig E 1994 *Phys. Status Solidi a* **142** K55
[8] Lang S and Muensit S 2006 *Appl. Phys.* A **85** 125
[9] Zhang Q, Chan H and Choy C 1999 *Composites* A **30** 163
[10] Chen G H, Xu H R and Jiang M H 2010 *J. Mater. Sci., Mater. Electron.* **21** 168
[11] Zubko P, Catalan G, Buckley A, Welche P and Scott J 2007 *Phys. Rev. Lett.* **99** 167601
[12] Hanzig J *et al* 2013 *Phys. Rev.* B **88** 024104
[13] Robertson J 2000 *J. Vac. Sci. Technol.* B **18** 1785
[14] Waser R and Aono M 2007 *Nat. Mater.* **6** 833
[15] Sawa A 2008 *Mater. Today* **11** 28
[16] Waser R, Dittmann R, Staikov G and Szot K 2009 *Adv. Mater.* **21** 2632
[17] Hanzig J, Zschornak M, Hanzig F, Nentwich M, Gemming S, Leisegang T and Meyer D C 2014 *J. Power Sources* **267** 700–5
[18] Menesklou W, Schreiner H J, Härdtl K H and Ivers-Tiffée E 1999 *Sensors Actuators* B **59** 184

[19] Schooley J F, Hosler W R and Cohen M L 1964 *Phys. Rev. Lett.* **12** 474
[20] Walter M G, Warren E L, McKone J R, Boettcher S W, Mi Q, Santori E A and Lewis N S 2010 *Chem. Rev.* **110** 6446
[21] Goldschmidt V M 1926 *Naturwissenschaften* **14** 477
[22] Eriksson A, Deleniv A and Gevorgian S 2003 *J. Appl. Phys.* **93** 2848
[23] Akimov I A, Sirenko A A, Clark A M, Hao J H and Xi X X 2000 *Phys. Rev. Lett.* **84** 4625
[24] Shirane G and Yamada Y 1969 *Phys. Rev.* **177** 858
[25] Cowley R, Buyers W and Dolling G 1969 *Solid State Commun.* **7** 181
[26] Li Y *et al* 2006 *Phys. Rev.* B **73** 184112
[27] Yuzyuk Y I 2012 *Phys. Solid State* **54** 1026
[28] Petzelt J *et al* 2001 *Phys. Rev.* B **64** 184111
[29] Uwe H, Yamaguchi H and Sakudo T 1989 *Ferroelectrics* **96** 123
[30] Pertsev N A, Tagantsev A K and Setter N 2000 *Phys. Rev.* B **61** R825
[31] Haeni J H *et al* 2004 *Nature* **430** 758
[32] Ehre D, Lyahovitskaya V, Tagantsev A and Lubomirsky I 2007 *Adv. Mater.* **19** 1515
[33] Lines M E and Glass A M 2001 *Principles and Applications of Ferroelectrics and Related Materials* (Oxford: Clarendon) ISBN 10: 019850778X
[34] Rabe K, Ahn C H and Triscone J M 2007 *Physics of Ferrelectrics A Modern Perspective* (Berlin: Springer)
[35] Byer R L and Roundy C 1972 *Ferroelectrics* **3** 333
[36] Garn L E and Sharp E J 1982 *J. Appl. Phys.* **53** 8974
[37] Lubomirsky I and Stafsudd O 2012 *Rev. Sci. Instrum.* **83** 051101
[38] Blanc J and Staebler D L 1971 *Phys. Rev.* B **4** 3548
[39] Mohapatra S K and Wagner S 2008 *J. Appl. Phys.* **50** 5001
[40] Kröger F A and Vink H J 1956 *Solid State Phys.* **3** 307–435
[41] Morin F J and Oliver J R 1973 *Phys. Rev.* B **8** 5847
[42] Shanthi N and Sarma D D 1998 *Phys. Rev.* B **57** 2153
[43] Cuong D D, Lee B, Choi K M, Ahn H S, Han S and Lee J 2007 *Phys. Rev. Lett.* **98** 115503
[44] Samara G 1966 *Phys. Rev.* **151** 378
[45] Bhalla A and Newnham R 1980 *Phys. Status Solidi* A **58** K19
[46] Bock O and Müller U 2002 *Acta Crystallogr.* B **58** 594
[47] Dove M T 2003 *Structure and Dynamics: An Atomic View of Materials* (New York: Oxford University Press) ISBN: 0-19-850677-5
[48] Lemanov V, Smirnova E, Syrnikov P and Tarakanov E 1996 *Phys. Rev.* B **54** 3151
[49] Hilton A D and Ricketts B W 1996 *J. Phys. D: Appl. Phys.* **29** 1321
[50] Oh S H and Jang H M 1999 *J. Appl. Phys.* **85** 2815
[51] Schlom D G, Chen L Q, Eom C B, Rabe K M, Streiffer S K and Triscone J M 2007 *Annu. Rev. Mater. Res.* **37** 589
[52] Noheda B, Zhong Z, Cox D, Shirane G, Park S and Rehring P 2002 *Phys. Rev.* B **65** 224101
[53] Ye Z G and Schmid H 1993 *Ferroelectrics* **145** 83
[54] Davis G, McKinney J, Broadhurst M and Roth S 1978 *J. Appl. Phys.* **49** 4998
[55] Fleury P and Worlock J 1968 *J. Phys. Rev.* **174** 613